International Journal of Applied Earth Observation and Geoinformation 120 (2023) 103342

Contents lists available at ScienceDirect

International Journal of Applied Earth Observation and Geoinformation

journal homepage: www.elsevier.com/locate/jag

On the potential of Sentinel-1 for sub-field scale soil moisture monitoring

T.C. van Hateren [a,b,*], M. Chini [a], P. Matgen [a], L. Pulvirenti [c], N. Pierdicca [d], A.J. Teuling [b]

[a] *Luxembourg Institute of Science and Technology, Department of Environmental Research and Innovation, 5 Av. des Hauts-Fourneaux, Esch-sur-Alzette, 4362, Luxembourg*

[b] *Wageningen University and Research, Department of Hydrology and Quantitative Water Management, Droevendaalsesteeg 2, Wageningen, 6708 PB, The Netherlands*

[c] *CIMA Research Foundation, Via Armando Magliotto, Savona, 17100, Italy*

[d] *Sapienza University of Rome, Piazzale Aldo Moro 5, Rome, 00185, Italy*

ARTICLE INFO

Keywords:
Soil moisture
High resolution
Experimental field study
Sentinel-1
C-band SAR

ABSTRACT

Soil moisture (SM) datasets at high spatial resolutions are beneficial for a wide range of applications, such as monitoring and prediction of hydrological extremes, numerical weather prediction, and precision agriculture. For large scale applications in particular, remotely sensed SM has advantages over in situ data because it provides gridded estimates and because it is less labour-intensive. However, until present, active microwave SM data have not been presented at their native spatial resolution, since the quality of these data is limited by speckle.

We explored the potential and limits of high spatial resolution of active microwave SM observations. We used a Sentinel-1 C-band SAR SM dataset at six spatial resolutions ranging from 20×20 to 120×120 m^2. This was compared to a closely spaced (20 m) in situ dataset collected on a non-irrigated agricultural field (±2.5 ha) in the Southeast of Luxembourg.

A comparison of the field and satellite datasets demonstrated how Sentinel-1 data with a high spatial resolution can be used to quantify temporal within-field SM variability. SM was accurately estimated at spatial resolutions of 60×60 m^2 and coarser, where the temporal correlation was found to be 0.67 and sub-field variations in SM were still detected. Spatial correlation was limited by the absence of SM variability within the field.

These results indicate that high spatial resolution SM estimates from Sentinel-1 data can be valuable for monitoring temporal SM variations within agricultural fields.

1. Introduction

Soil moisture (SM) is an important variable in the water cycle as it controls the exchange of both water and energy between the land surface and the atmosphere (Seneviratne et al., 2010; Vereecken et al., 2014), in particular during droughts and heatwaves (Miralles et al., 2019; Teuling, 2018). SM observations at high spatiotemporal resolutions can improve numerical weather prediction (Lagasio et al., 2019b,a), serve applications such as precision agriculture (Vereecken et al., 2014), and enhance monitoring and prediction of hydro-meteorological disasters (Wood et al., 2011; Bierkens et al., 2015; Peng et al., 2021; Vergopolan et al., 2021).

In situ SM observations, though accurate, are still scarce because of costs and man-hours involved in acquisition, installation, and maintenance of sensors. Furthermore, observations are effectively made at point scale and thus lack spatial representativeness and spatial coverage (Teuling et al., 2006; Seneviratne et al., 2010; Crow et al., 2012; Babaeian et al., 2019; Peng et al., 2021). Remotely sensed SM products, on the other hand, are less labour intensive and provide a gridded estimate of SM with a large spatial coverage. Consequently, these data can be assimilated in hydro-meteorological models directly (Hostache et al., 2020).

Several global or continental gridded SM datasets are currently available (Peng et al., 2021), such as ESA CCI soil moisture (Gruber et al., 2020), NASA USDA Global Soil Moisture Data, and Copernicus Global Land service Surface Soil Moisture (CSSM). These open data can be very useful for modelling studies thanks to their large-scale coverage. However, their spatial resolution (0.25 deg, 0.25 deg, 1 km, respectively) does not yet allow for SM monitoring at the scale of

* Corresponding author at: Wageningen University and Research, Department of Hydrology and Quantitative Water Management, Droevendaalsesteeg 2, Wageningen, 6708 PB, The Netherlands.
E-mail address: tessa.vanhateren@list.lu (T.C. van Hateren).

https://doi.org/10.1016/j.jag.2023.103342
Received 14 February 2023; Received in revised form 3 May 2023; Accepted 3 May 2023
Available online 24 May 2023

individual fields or even at the sub-field scale that is most relevant for (precision) agriculture.

SM can be observed at sub-field scales with the use of active microwave data, as provided for instance by the Sentinel-1 (S1) satellites. Active microwave sensing has the benefits of a high native spatial resolution, and can be performed day and night and under all weather conditions (Babaeian et al., 2019). On the other hand, SM retrieval accuracy is hampered by uncertainties caused by speckle, surface roughness, the presence of vegetation, water bodies, and frozen soils. These uncertainties have to be accounted for in the SM retrieval and might limit the effective spatial resolution at which SM can be inferred.

An integral part of any SM retrieval is the forward model that predicts the backscatter for given surface conditions. Multiple forward models exist, such as the physical Advanced Integral Equation Model (Fung et al., 1992), the Water Cloud Model (Attema and Ulaby, 1978), and the semi-empirical Oh model (Oh, 2004). The Oh model has been applied successfully in many SM retrieval studies (e.g. Choker et al., 2017; Pulvirenti et al., 2018; Wang et al., 2018; Ezzahar et al., 2020). Retrieval algorithms are even more numerous, with different underlying methods to account for uncertainties, such as change detection (e.g. Wagner et al., 1999; Balenzano et al., 2011; Bauer-Marschallinger et al., 2019), artificial neural network (Del Frate et al., 2003; Elshorbagy and Parasuraman, 2008; El Hajj et al., 2017; Hachani et al., 2019), or multiple least squares (Mattia et al., 2009; Kim et al., 2014; Pierdicca et al., 2014; Zhu et al., 2019) methods.

In addition to the retrieval process, evaluating the accuracy of SM retrievals with high spatial resolutions poses it own challenges (Gruber et al., 2020). Since in situ SM data lack spatial representativeness, the reference in situ point dataset must be of sufficient spatial density (i.e. small spacing, Western and Blöschl, 1999) and account for sampling uncertainty. Big efforts have been made to monitor SM and to make these datasets publicly available, such as in the International Soil Moisture Network (ISMN, Dorigo et al., 2021) or during numerous ground validation experiments (SGP97,NAFE'06,SMAPVEX12, 16, SMAP Cal/Val Colliander et al., 2015, 2017, 2019). Unfortunately, currently available in situ datasets like these do not have sufficiently small spacing and/or their measurement period does not overlap with S1 acquisitions. Dedicated field experiments using robust and intensive spatio-temporal sampling are required for a fair analysis of a satellite dataset on multiple high spatial resolutions: the pixel-average in situ SM must be known at all of the studied resolutions. For that reason, a field campaign with small spacing was set up in Luxembourg, where topography is limited and a strong seasonality in surface SM exists (Matgen et al., 2012).

We hypothesise that even S1 data at its native spatial resolution contains relevant information on sub-field moisture conditions and aim to find the minimal spatial resolution at which speckle still allows for accurate SM estimates. For this purpose, we use a multitemporal pixel-based algorithm introduced by Pulvirenti et al. (2018) to retrieve SM at different high spatial resolutions (20×20 – 120×120 m^2). The S1 retrieved SM dataset was then evaluated against an in situ dataset whose spacing matches the S1 native spatial resolution. This dataset resulted from a field campaign on a non-irrigated agricultural field of ±2.5 ha in the Southeast of Luxembourg during 2020 and 2021. The evaluation for the entire time period is supplemented with a case study, entailing a short period with strongly varying SM conditions. We then discuss benefits and limitations of SM monitoring at these high spatial resolutions.

2. Study area and data

2.1. Study area

We focused our study on a non-irrigated agricultural field (±110 by 250 m) in South-eastern Luxembourg (Fig. 1). Luxembourg is located in Central Western Europe and marked by its moderate climate. The

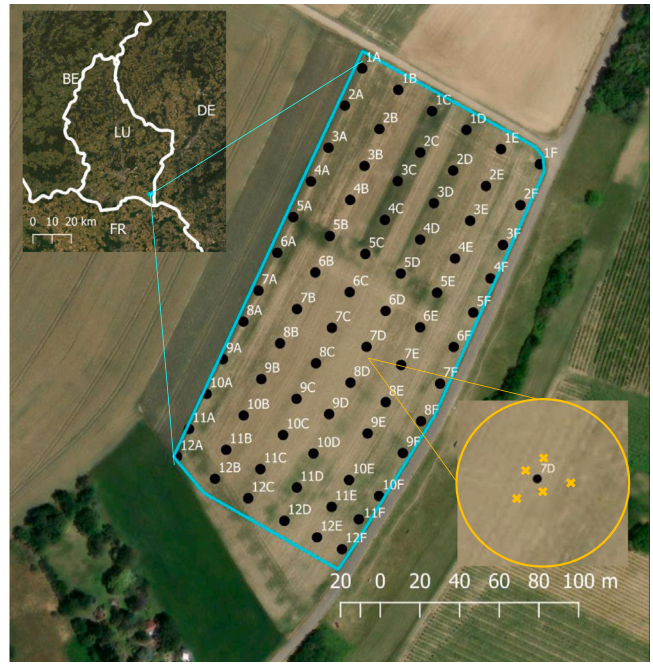

Fig. 1. Location of the study area and the sampling points for the reference dataset (centre at 6.31774°E, 49.51109°N). At each of the 72 sampling points, five TDR measurements were taken, of which an example lay-out is given in the circular inset. In total, 360 TDR measurements were thus taken per measurement day.

field's soil can be classified as a moderately gleyic clay on a calcareous substrate, according to the Luxembourgish Geoportal. Their high spatial resolution elevation data shows a slight slope in the field from the northern to the southern corner (±9 m elevation difference, Fig. A.14).

This specific field was chosen for its close proximity to a permanent meteorological station, and because of its availability for in situ measurements over a long time period. The long time period was necessary in order to obtain measurements at a large range of moisture conditions. Vegetation state in the field varied throughout the measurement period (Fig. A.13): during the 2020 growing season maize covered the field, and winter wheat was sown in the fall of 2020. The winter wheat grew to a few cm before low temperatures stagnated their growth, hence a slight coverage of vegetation was present in the 2020–2021 winter season. Growth then continued from March onward.

2.2. In situ data

In situ SM data were gathered in the field 38 times between March 2020 and June 2021 (with a gap in between April and September 2020, Fig. 2), on all days coinciding with S1 overpasses and under varying SM and weather conditions. On each campaign day, five SM measurements were taken at each location on a 12×6 grid, with a grid spacing of approximately 20 meters (Fig. 1). SM was measured with a FieldScout Time Domain Reflectivity (TDR) 350 with 3.8 cm metal pins. These short pins were used to have a similarly superficial measurement depth as the S1 retrieved SM estimates. Additionally, on some of the field days, 12 volumetric soil samples were taken at random TDR sampling locations. The soil samples were then weighed, oven-dried for 24 h, and weighed again to determine the soil bulk density and the SM. These SM values were used to calibrate the TDR measurements. Finally, on field days, vegetation height was determined at various locations in the field to be compared with NDVI data. No roughness measurements were performed.

At a nearby permanent meteorological station (6.32893°E, 49.49475°N), hydrometeorological variables such as SM (at 10, 20, 40, 60 cm depth), air temperature, and precipitation are measured continuously. These data were used in the analysis, where meteorological conditions in the field were assumed to be similar to conditions at the station.

2.3. Satellite data

Amongst the presently available active microwave sensors (see e.g. Babaeian et al. (2019)), S1 data is the most promising: ESA freely provides S1 data at a 20 × 22 m^2 resolution (ESAS̃entinelÕnline, 2023), keeps the satellites under a strict acquisition scenario, and is expected to continue these observations for the next few decades (Bauer-Marschallinger et al., 2019; Peng et al., 2021). Every S1 orbit provides backscatter data at the exact same location every 6 days. Data from two different descending orbits (RO37 and RO139) were retrieved, with an average local incidence angle (LIA) of respectively 33.5° and 42.1° over the study area. S1 data were downloaded in Level-1 high resolution Interferometric Wide (IW) swath ground-range detected (GRD) format in VV polarisation for the days indicated in Fig. 2.

As an indication of vegetation state over the study area, Normalized Difference Vegetation Index (NDVI) data were used. These data were derived from Level-2 optical data from the Sentinel-2 (S2) satellite. Although each S2 orbit has a five day revisit frequency, fewer data were available for this study because only images that are cloud-free over the study area were used. Moreover, only data from the 108 orbit were used. Data were finally retrieved on days shown in green in Fig. 2.

The 100 × 100 m^2 resolution Corine Land Cover map 2018 was used as land cover input data for the soil moisture retrieval algorithm. Although this is at a lower spatial resolution than the other input data, the results of the present study are not affected since the studied field is characterised under the same land cover type. Finally, the digital elevation model (DEM) over the study area was extracted from the Shuttle Radar Topography Mission (SRTM) (EROS, 2017).

3. Methods

3.1. Pre-processing

Prior to the analyses, the five TDR measurements at each sampling location were averaged to obtain a single value per location. Then, raw TDR data were calibrated making use of the volumetric SM samples (Fig. 3). A linear relationship existed between the two measurement types, so that a linear transformation could be applied to all raw TDR data: TDR=0.098+0.97 ·rawTDR. The analyses described here were performed with these calibrated TDR data.

S1 GRD backscatter intensity data (σ^0) were preprocessed with ENVI SARscape. The precise orbit files were applied, thermal noise was removed, and data were radiometrically calibrated, multi-looked (4 pixels in the range direction) and geocoded using the STRM DEM on the WGS 84/UTM zone 32N coordinate system to finally obtain a square pixel of 20 × 20 m^2. The LIA and the slope over the study area were also extracted using the SARscape tool.

S2 optical data was converted to NDVI data with ESA's Sentinel Application Platform (SNAP) 7.0 tool.

3.2. Soil moisture retrieval

3.2.1. The retrieval algorithm

The MUltitemporal LEast Square Moisture Estimator (MULESME) algorithm (Pulvirenti et al., 2018) is a multitemporal physically-based algorithm. It has been evaluated previously and has been shown to accurately estimate SM on a pixel-by-pixel basis (Pulvirenti et al., 2018). The inversion of SM content and surface roughness is performed in each pixel using an least-square-errors approach. The algorithm assumes that SM content changes considerably faster than surface roughness, and in doing so reduces the ill-posedness of the soil moisture retrieval problem (Pierdicca et al., 2014). If only one image was used, there would be two unknown values (soil moisture and roughness) and one known value (backscatter) per pixel. By using five images over a period with constant roughness, the number of knowns increases to five, but the number of unknowns only increases to six. Over shorter periods, the constant roughness assumption is more likely to be valid. Over longer periods, the estimation accuracy is higher but computation time increases dramatically. The use of five images is thus a compromise between accuracy and efficiency (Pierdicca et al., 2014). For more information on the algorithm and its underlying theory, we refer to Section 3.2.2, Pierdicca et al. (2014) and Pulvirenti et al. (2018).

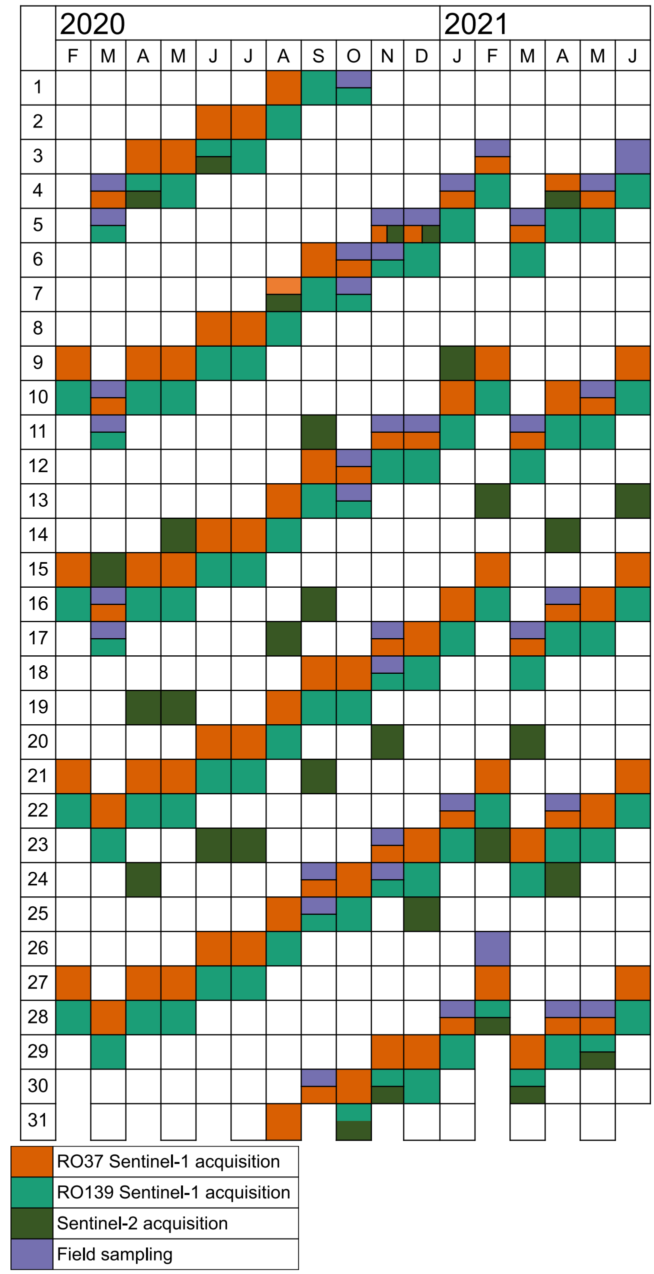

Fig. 2. Overview of the timing of S1 (RO37, RO139), S2, and in situ data acquisitions.

In comparison to other retrieval algorithms, the first advantage of the MULESME algorithm is that it is versatile in its application since it can be run on a varying spatial resolution 'on demand'. Secondly, the algorithm does not require a calibration for every pixel since the underlying empirical equations have been calibrated. This

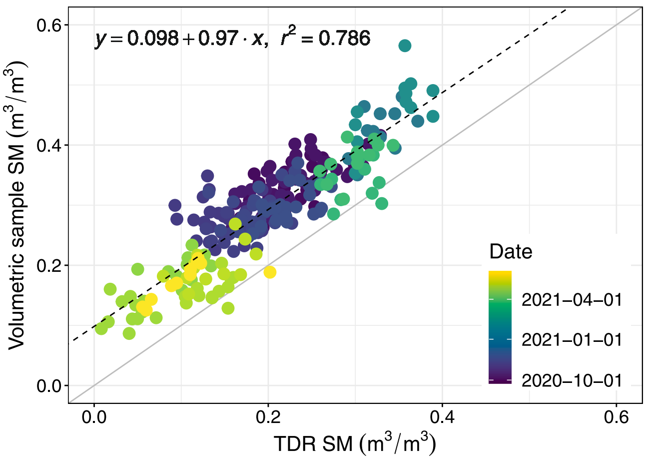

Fig. 3. A comparison of the two in situ measurement approaches. The x-axis shows the SM content as measured by the TDR device, and the y-axis the SM content as derived from the soil samples. The dashed line shows the linear regression model and the solid line follows the 1:1 line.

pixel-by-pixel calibration is required for other methods relying on the availability of a long record of backscatter data (Bauer-Marschallinger et al., 2019). Thirdly, MULESME implements a multitemporal approach which enables us to mitigate the uncertainty caused by roughness.

The MULESME algorithm first resamples all input data (LIA, σ^0, NDVI, slope, land cover) to the specified spatial resolution. Then, each σ^0 pixel is corrected as described in Section 3.2.2. SM and surface roughness are finally inverted, making use of a look up table (LUT) that contains 7956 unique combinations of backscatter, SM, roughness and LIA based on the Oh forward model using a least-squares minimisation approach. The use of a LUT is considerably faster than computing the forward model repeatedly (Pulvirenti et al., 2018).

One MULESME run finally results in five S1 SM maps, and a unique roughness map. The algorithm was run with a temporally moving window of five σ^0 images: for each new run, one new σ^0 image was added and the eldest one was removed from the computation (Fig. 4). This was repeated until all the S1 images indicated in Fig. 2 were processed. The two different orbits were processed separately to ensure constant geometrical acquisition conditions (e.g. the same incidence angle) between the five consecutive backscatter images. Then, the SM maps were further processed (Section 3.3) and the roughness maps could be analysed immediately. Although no site-specific calibration was performed, estimated roughness conditions did approach their boundary conditions (Fig. 5) and their temporal dynamics were as expected, with large changes occurring only during sowing and harvesting of the crops (Bousbih et al., 2017).

3.2.2. Minimising retrieval uncertainties

Several uncertainties in the retrieval have to be accounted for in the analysis, most notably speckle, surface roughness, frozen soils and the presence of vegetation.

Speckle in the σ^0 image is caused by inhomogeneities in the scattering natural target and results in grainy backscatter images (Lee, 1986). Speckle is generally reduced with spatial aggregation (e.g. Attarzadeh et al., 2018; Tripathi and Tiwari, 2020) or dedicated speckle filtering (e.g. Schönbrodt-Stitt S. Ahmadian et al., 2021). In this case, we only multi-looked the image 4 times in the range direction because we aimed to catch SM variation at a high spatial resolution. Applying a more rigorous speckle filter could hamper this since variations in backscatter could be interpreted as speckle rather than SM variation.

Surface roughness influences the scattering of microwaves and is corrected by assuming that moisture conditions change faster than roughness conditions (Pulvirenti et al., 2018).

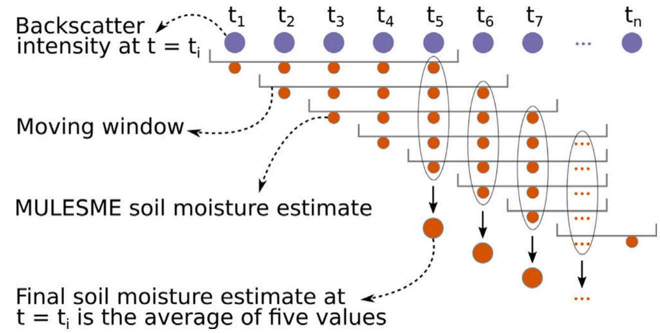

Fig. 4. Graphical illustration of the moving window approach.

Frozen soils decrease dielectric constant of the soil substantially (de Rosnay et al., 2006; Hallikainen et al., 1985) and are therefore flagged and removed after retrieval. Images acquired at a time when air temperatures at the meteorological station dropped below 2 °C were excluded from the computation of the temporal performance metrics. They were included in the spatial analysis because in that case the data show how frozen soils affect the retrieval, but do not influence performance metrics for the entire time period.

Vegetation water content influences the scattering of the microwave signal and is often corrected in the retrieval as a dynamic parameter that changes in time, as does MULESME. It uses NDVI as a proxy for Plant Water Content (PWC), which is used to correct the σ^0 images for signal scattering by vegetation following Section 2.3 in Pulvirenti et al. (2018). PWC is derived from the NDVI images with an empirical equation that depends on the land cover of the pixel. The studied field is located in an area classified as agricultural, and as such, the conversion follows Eq. (1) (Chan et al., 2011).

$$\mathrm{PWC} = (1.9134 \cdot \mathrm{NDVI}^2 - 0.3215 \cdot \mathrm{NDVI}) + 3.5 \cdot \frac{(\mathrm{NDVI} - 0.1)}{0.9} \tag{1}$$

σ^0 is corrected for the vegetation signal if $0.25\ \mathrm{kg/m^2} < \mathrm{PWC} \leq 5\ \mathrm{kg/m^2}$. When $\mathrm{PWC} > 5\ \mathrm{kg/m^2}$, the pixel is masked from the backscatter image.

Backscatter pixels that are higher than −2 dB or lower than −18 dB after vegetation correction are masked out, since these values lie outside of the range of backscatter values under which soil moisture can be accurately retrieved (Pulvirenti et al., 2018).

3.3. Post-processing

During post-processing, any MULESME runs that included a known roughness change (e.g. due to ploughing in Oct 2020, Fig. A.13) were removed from the analysis. Moreover, SM images were averaged to create a single ensemble mean per overpass day (Fig. 4, Zhu et al., 2020; Lee et al., 2021). A combination of a moving window and this averaging has two advantages. First, a moving window allows us to work with a shorter set of images so the hypothesis of constant roughness is more reasonable. Second, the averaging reduces the uncertainty in the SM estimate by exploiting more backscatter measurements.

Then, lower spatial resolution SM maps were created (i.e. 40×40, 60×60, 80×80, 100×100, $120 \times 120\ \mathrm{m^2}$) by multi-looking the retrieved $20 \times 20\ \mathrm{m^2}$ SM map. Although multi-looking before SM retrieval is a more common approach to reduce speckle, this approach leads to the mixing of pixels that potentially have different SM, vegetation and roughness conditions. This could hamper SM retrieval, especially at high spatial resolutions. By retrieving SM first, and multi-looking second, different conditions are accounted for in the retrieval. Both this approach and the inverse (i.e. retrieving after multilooking) have been tested in a synthetic experiment and over the study area, of which the results are presented in van Hateren et al. (2023). They showed that multi-looking after retrieval results in higher retrieval accuracy.

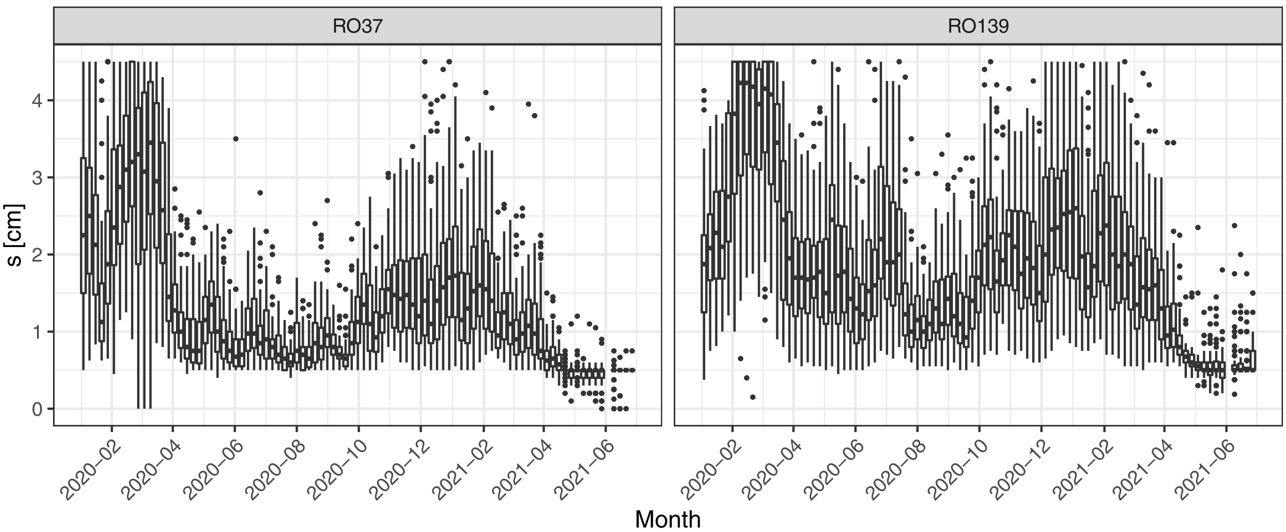

Fig. 5. Illustration of the temporal dynamics of inferred roughness during the field campaign, provided in root mean square surface height [cm]. Boxplots with their minimum, 25th quartile, median, 75th quartile, maximum, and outliers as dots, are provided for every overpass day. The left panel shows results for RO37 and the right panel for RO139.

3.4. Data analysis

The accuracy of the SM images was evaluated by comparing the S1 retrieved SM maps to the in situ reference data at all six derived spatial resolutions. To that end, the in situ SM data were converted from point to raster data by averaging all TDR estimates located in the overlying pixel. Then, S1 retrieved and in situ SM images were compared to analyse the satellite's ability to capture the spatial SM variability.

We also computed two performance metrics to quantify the accuracy and error of the SM retrieval at the six different spatial resolutions: spatial and temporal Pearson correlation coefficient (r, Eq. (2)) and spatial and temporal unbiased root mean square error (ubRMSE, Eq. (3)). The RMSE quadratically penalises any deviation from in situ observations, but is sensitive to any bias in the data. The ubRMSE removes that from the equation and is thus useful for SM datasets, since in their application, an accurate estimate of the temporal SM variation is more relevant than its exact value (Reichle et al., 2007; Entekhabi et al., 2010). The Pearson correlation is a useful addition as it quantifies the agreement in space or time between the satellite dataset and the in situ dataset.

$$r = \frac{\sum_{i=1}^{n}(y_i - \overline{y})(x_i - \overline{x})}{\sqrt{\sum_{i=1}^{n}(y_i - \overline{y})^2}\sqrt{\sum_{i=1}^{n}(x_i - \overline{x})^2}} \tag{2}$$

$$\text{ubRMSE} = \sqrt{\frac{1}{n}\sum_{i=1}^{n}((y_i - \text{ME}) - x_i)^2} \tag{3}$$

$$\text{ME} = \frac{1}{n}\sum_{i=1}^{n} y_i - x_i \tag{4}$$

In Eqs. (2) – (4), y stands for the estimated SM, x for the in situ observed SM, n for the number of samples and i for each individual pair of observations.

3.5. Comparison with copernicus surface soil moisture

To confirm the suitability of the MULESME algorithm for SM retrieval, we not only include a comparison of MULESME SM to a field study, but also to results of the more widely used TU Wien Change Detection model (Bauer-Marschallinger et al., 2019). This model has been used by the Copernicus Global Land Service to operationally retrieve global SM from S1 on a 1×1 km^2 resolution (CSSM dataset, https://land.copernicus.eu/global/products/ssm). Whereas MULESME retrieves absolute SM based on the forward Oh model, the TU Wien model interprets changes in backscatter as changes in SM and thus ends up with a relative estimate of SM in % saturation.

We performed a comparison with MULESME SM aggregated to the same spatial resolution and with average field in situ values. All three datasets were filtered for frozen soils and adverse vegetation conditions. We hypothesised that MULESME SM trends align with TU Wien SM trends, and assume that will be the same on higher spatial resolutions. Conclusions drawn in applying this method will therefore likely be transferable to the use of a different algorithm.

4. Results

4.1. Soil moisture conditions during field campaign

Data for the full time period are provided in the appendix.

Although a temporal average of SM (Fig. 6) shows that SM was not homogeneous in the field, spatial variability within the field was considerably smaller than temporal variability. On days coinciding with the 139 overpass (RO139), the field was slightly wetter than on days coinciding with the 37 overpass (RO37). A wetness gradient in the field from northwest to southeast is visible in the high resolution satellite images (i.e. 20, 40, 60 m), but it can no longer be detected in the images with a larger pixel size. The gradient is comparable between the in situ and satellite data and between the RO37 and RO139 data. However, a clear bias exists in the results: the temporally averaged TDR values range from 0.30 to 0.40, whereas the satellite values range from 0.16 to 0.26.

4.2. Temporal metrics

The bias in average SM conditions is also apparent in the temporal SM dynamics (for the complete dataset we refer to the appendix: Fig. B.15,B.16). The centre panel in Fig. 7 shows the S1 retrieved SM time series, as well as air temperature and daily precipitation at the permanent station at the time of the satellite overpass. The time series show that the bias between satellite and in situ data is slightly more severe in the RO37 data than in the RO139 data. At the same time, the temporal evolution is generally well described in the satellite data: The impact of the presence and absence of precipitation can be seen in increasing and decreasing SM conditions, in satellite as well as in situ data.

Differences in performance can be observed for different field conditions. Some examples are highlighted in Fig. 7. In periods highlighted in

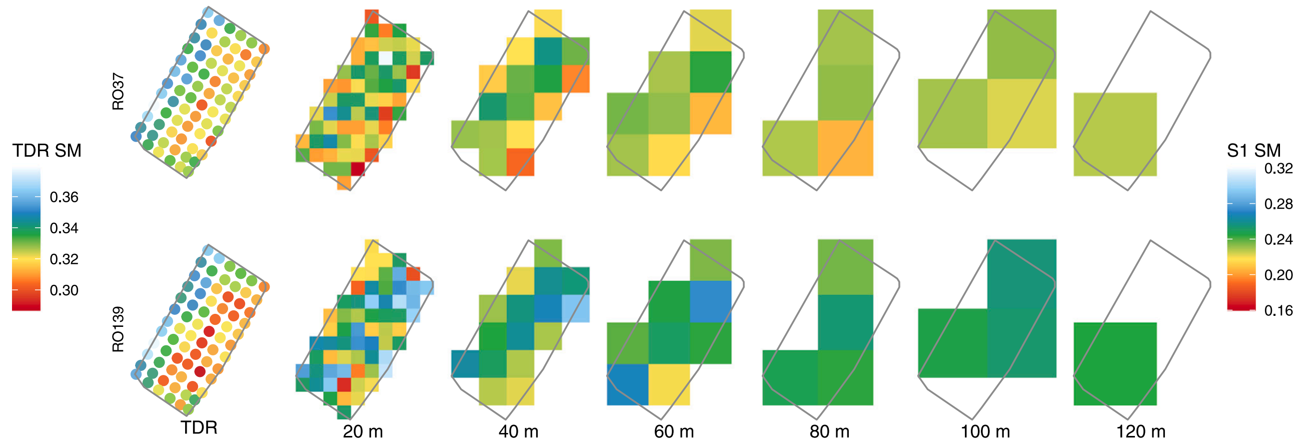

Fig. 6. Temporal average of SM content throughout the field measurement campaign. The points in the first column show the in situ TDR data, and the pixels in the remaining columns show the S1 SM data on six different spatial resolutions. The two rows show the data for the two different orbits, and thus for different days in the measurement period (Fig. 2). Data were removed from the analysis when temperatures were below 2 °C, when standing water was observed on the field and when vegetation hampered the SM retrieval (Section 4.2).

green (Fig. 7a, b, c, e), the S1 SM estimates follow the in situ temporal dynamics rather well. The photos taken in the field during these periods show that soils were bare or covered with only minimal amounts of vegetation. Moreover, the meteorological conditions were moderately wet and moderately warm, with temperatures rarely dropping below 2 °C. A bias in the results still persists, albeit less so in October 2020 (Fig. 7b). In that period, temperatures stayed above 5 degrees and precipitation occurred almost daily. In contrast, January 2021 (Fig. 7d) showed especially challenging conditions for SM retrieval. Air temperatures were very low (<2 °C) for the first half of the month. This led to frozen soils in mid January, when satellite estimates of SM dropped to values of around 0.1, a clear underestimation of actual moisture conditions. At the end of the month, frozen soils made way for standing water on the field. This caused specular reflection that decreased the backscatter intensity and again led to an underestimation of SM conditions.

In April–May 2021 (Fig. 7f), vegetation hampered accurate SM retrievals. S1 SM estimates dropped to extremely low values rapidly before in situ conditions reflected this drop. S1 SM estimates did also not reflect the expected signal after precipitation in the beginning of May. The reduction in estimation accuracy in this period coincides with a period of large uncertainty in roughness estimates (Fig. 5), that are suddenly extremely low starting from mid April 2021, likely due to the presence of vegetation. The vegetation attenuates the σ^0 signal, and the algorithm is unable to distinguish this attenuation from surface scattering. Hence, the backscatter is low not because of low SM, but because of the small part of the signal that reaches the surface in the first place.

Based on this analysis, several conditions that affect the performance of S1 SM retrieval were filtered out before computing the temporal metrics:

- days where air temperatures dropped below 2 °C;
- days where standing water was observed; and
- days during the height of the growing season (after 2021-04-15).

After filtering, 22 days with TDR measurements remained, 12 for the RO37 data and 10 for RO139.

The temporal metrics for the two different orbits are visualised in Fig. 8(a). The smaller amount of in situ data for RO139 leads to non-significant correlations more often than for RO37: only at resolutions lower than 80 m, the majority of pixels has a significant Pearson correlation ($P<0.05$). For the RO37 data, this is already the case at 40 m. The temporal Pearson correlation (r, Fig. 8(a)) is higher in the RO37 data for high spatial resolutions, but for low spatial resolutions, the RO139 data perform better. The RO37 20 m resolution has a spatially averaged temporal r with the in situ data of 0.39 (or 0.66 for significant pixels). At 40 m resolution, the average correlation already improves to 0.59 (or 0.68). The improvement in r stagnates after 60 m with a value of 0.67 (0.69) and does not get higher than 0.69 at a 100 m resolution. In the RO139 data, r improves until a lower resolution, peaking at 0.76 at a 100 m resolution. Comparing the different pixels within each resolution, spatial variation is limited for the RO37, except on the 20 m resolution. For the 139 orbit, a higher spatial variation exists, with higher correlations occurring in the northern part of the field.

The temporal ubRMSE gives an indication how different the S1 SM estimates are from the in situ SM observations (Fig. 8(b)). At lower spatial resolutions, the value decreases slightly from 0.09 to 0.05 (RO37) or 0.04 (RO139). Spatial variation in the ubRMSE is especially apparent in the 20 m resolution images and is more pronounced in the 139 than the 37 orbit. In both cases, spatial variability decreases as spatial resolution decreases.

4.3. Spatial metrics

Spatial metrics were computed for the entire field campaign, hence including the days that were characterised by unfavourable retrieval conditions. They are shown in Fig. 9 for each day on which field data were collected, together with their averages over the entire time period. To distinguish between favourable and less favourable conditions, temperature and vegetation conditions are indicated in different shapes and colours in the plot, respectively. Spatial metrics could not be computed for the 120 m resolution because there was only one pixel at this size that had more than 50% of its area located in the field (see Fig. 8). It should also be noted that at lower spatial resolutions, fewer pixels can be analysed and so the chances of finding a significant correlation decrease.

The average spatial r (printed in grey in Fig. 9) over the field is low. In the case of RO37 (upper panels), r increases as the spatial resolution decreases, with its maximum at 0.232 at 100 m resolution. For RO139 (lower panels), no clear trend exists between the average r and spatial resolution. The highest r does occur at the lowest spatial resolution, with a value of 0.062. In contrast, the average ubRMSE clearly improves with increasing spatial resolution for both orbits. For both orbits ubRMSE drops below 0.04 at 60 m resolution, further decreasing to their respective minima at 100 m (RO139: 0.016; RO37: 0.017). Differences in performance between the orbits are mostly visible at high resolutions (up to 60 m), where RO37 outperforms RO139.

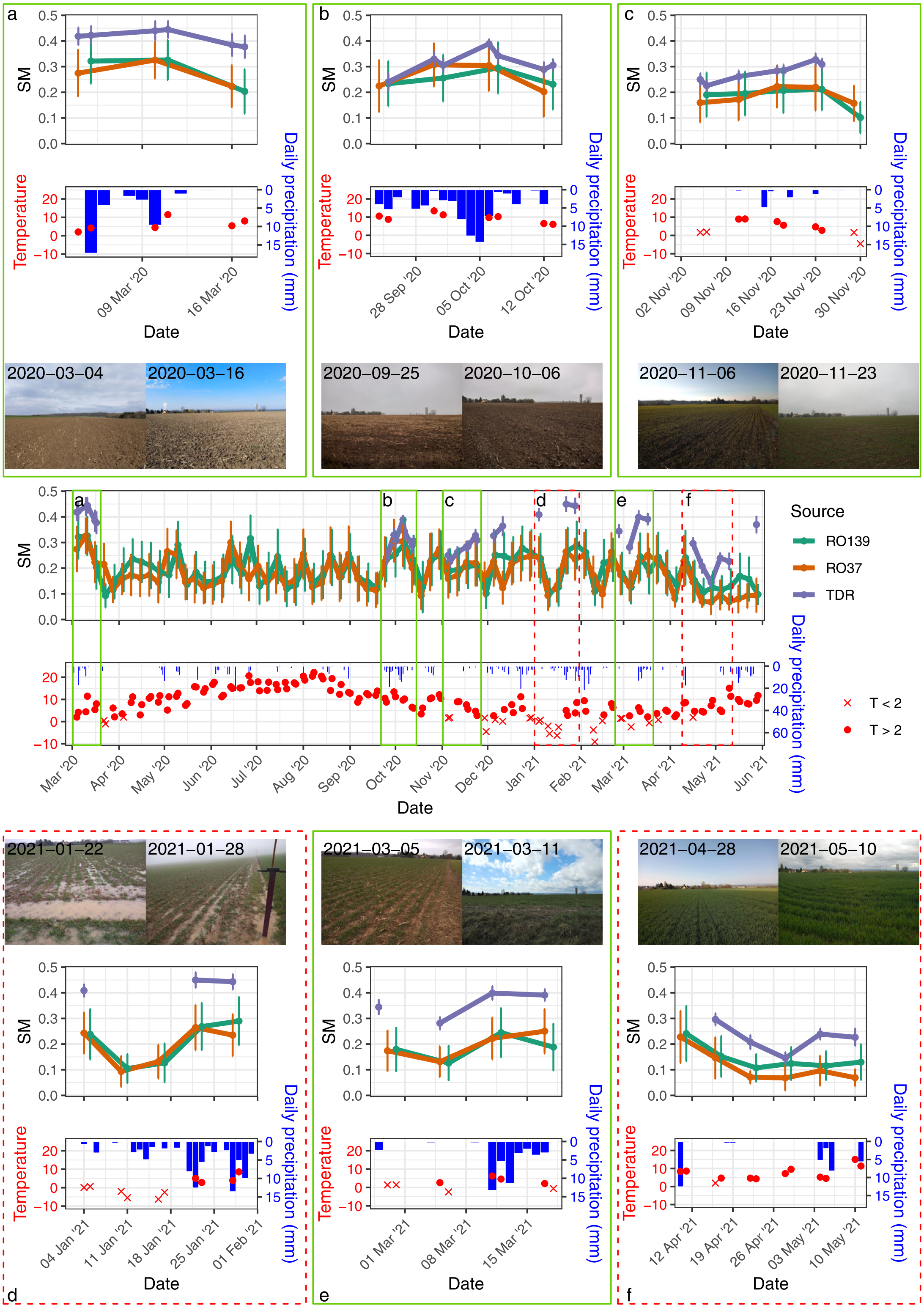

Fig. 7. Illustration of the temporal SM dynamics during the field campaign. The centre panel shows TDR (purple) and S1 (green, orange) time series through the 2020–2021 winter and beginning of the 2021 growing season, with error bars indicating the standard deviation, and meteorological conditions: daily precipitation in blue and air temperature at the time of overpass in red. Subplots a, b, c, d, e, and f zoom in on periods that are discussed in the manuscript. (For interpretation of the references to colour in this figure legend, the reader is referred to the web version of this article.)

The separate shapes in Fig. 9 show the spatial performance metrics for each day on which data were collected. The low average *r* discussed earlier is clearly not caused by outliers, since on most days the correlation is rather low, especially at high spatial resolutions. Moreover, in only a handful of cases the correlation was found to be significant ($P<0.05$), shown by the filled shapes. In RO37, a significant correlation was found on only two or three days for all studied spatial resolutions. In most cases, these significant correlations were found to be positive. Negative significant correlations only occur for temperatures below 2 °C, as shown by squares in the figure. For the RO139 on the other

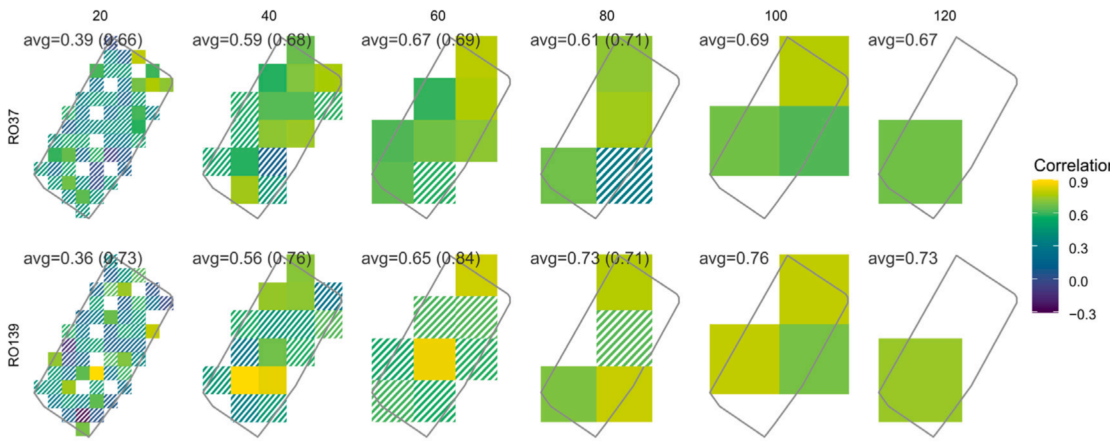

(a) Pearson correlation per pixel.

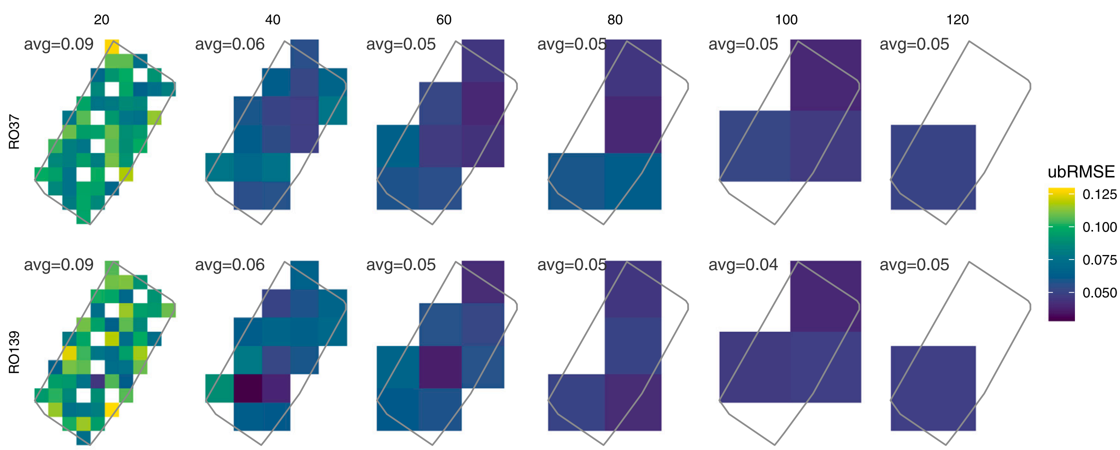

(b) Unbiased root mean square error per pixel.

Fig. 8. Temporal performance metrics between S1 SM and in situ data, for all six different spatial resolutions studied here. Pixels with non-significant correlation values are dashed. The grey text shows the metric averaged over the entire field, and the correlation for the significant correlations only are given between brackets. Data were removed from the analysis when temperatures were below 2 °C, when standing water was observed on the field and when vegetation hampered the SM retrieval (Section 4.2).

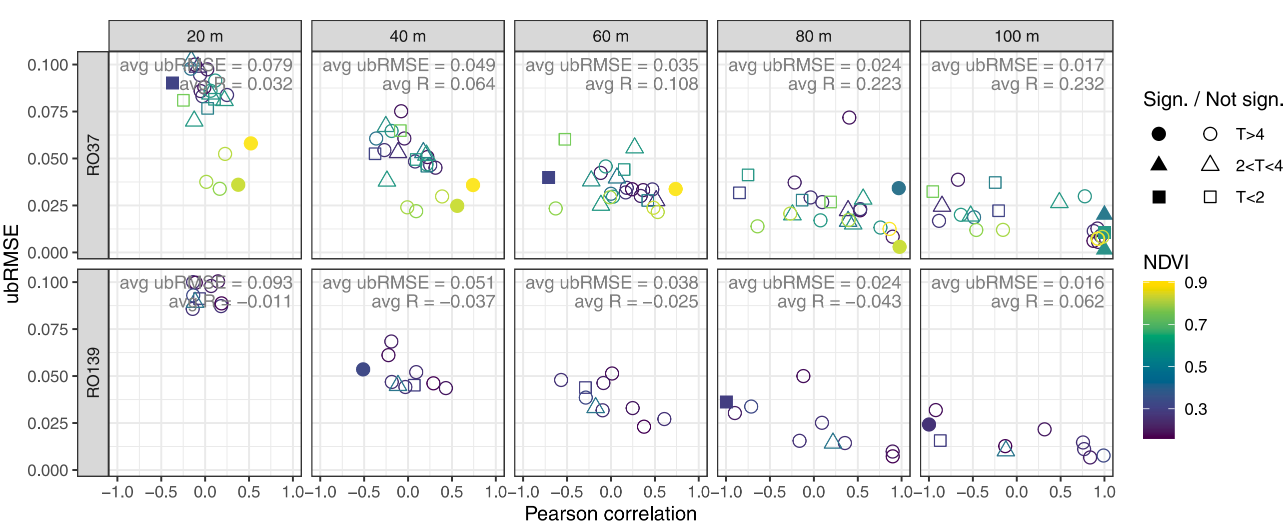

Fig. 9. Spatial correlation and unbiased RMSE on each day of the field campaign, for different spatial resolutions (m). Colours show the value for field-averaged NDVI on that measurement day. Filled shapes indicate that the correlation was significant (P<0.05) and shapes indicate the temperature range at the time of overpass. The text in grey shows the average *r* and ubRMSE. At a 120 m resolution, only one pixel is present in the field, so no values for spatial correlation exist and ubRMSE equals zero by definition.

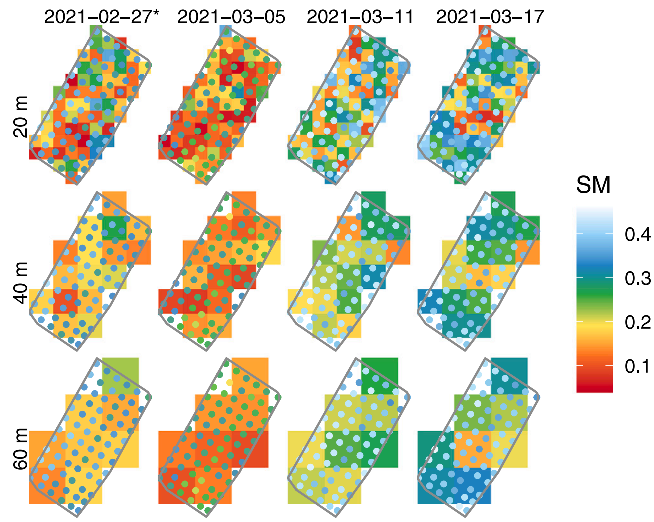

Fig. 10. Spatiotemporal SM dynamics in the field in February–March, 2021 at a 20, 40, and 60 m spatial resolution. The S1 SM is shown as pixels in the back and the TDR measurements are plotted as points on top.
*Due to a lack of TDR data on 2021-02-27, TDR data from 2021-02-26 are shown.

hand, in all cases where correlation is significant, it is negative. Both orbits show an increasing variability of r at decreasing spatial resolutions, shown by the spreading of values over the x-axis. Interestingly, the ubRMSE shows an opposite trend in RO37: spread in the y-direction decreases at lower resolutions. This trend is not visible in RO139. For both orbits, the ubRMSE is lower than 0.05 for most days in 60, 80 and 100 m resolutions, but generally higher in 20 and 40 m resolutions.

Only one clear high ubRMSE outlier in the data exists at the 80 m resolution for orbit 37. Low outliers are visible in the 20 and 40 m resolutions at RO37, interestingly on days with high NDVI values. Judging from the temporal analysis in Section 4.2, this seems to be a coincidence rather than a result with a physical basis: both increased vegetation and decreasing water content result in the same change in backscatter and occurred simultaneously in the early summer of 2021. In terms of temperature, correlations are often negative when temperatures were below 2 °C (squares in Fig. 9). No substantial difference was found between the spatial metrics on days where temperature was between 2 and 4 °C (triangles) and days where temperature was higher than 4 °C (circles).

4.4. Case study

Both the temporal and spatial analysis indicated that differences in retrieval accuracy exist between individual days. Even though spatial correlations are generally low due to the low variability in the field, we expect that under favourable field conditions, MULESME is able to capture temporal dynamics on a high spatial resolution. In this case study, we zoom in to a period with favourable field conditions and a clear temporal variation in SM (Fig. 7): February–March 2021. This analysis is performed for the RO37 data only, since higher performances were found at higher spatial resolutions compared to the RO139 data.

Fig. 10 shows that the first two studied days are drier than the last two days. The biggest change in SM is observed between the 5th and the 11th of March. Temporal in situ SM trends are accurately represented in S1 SM conditions: wetter in situ conditions correspond with wetter S1 SM conditions and vice versa. This is not true for all spatial resolutions. At a 20 m resolution, the satellite retrieval shows spatially varying SM in the field that is not present in the in situ data. At lower spatial resolutions, the agreement between different pixels in space improves, and patterns in situ data are better represented in the satellite data. However, the earlier identified bias is still visible.

To further test whether temporal trends are accurately represented in the MULESME output, we plotted the temporal variation in SM content in the field for the 20, 40, and 60 m resolution (Fig. 11). The satellite data does bear a distinct resemblance to the in situ data. The daily variations show that trends found in spatially aggregated in situ data are well visible in satellite data with high a spatial resolution. This is especially true for the centre date pair, when SM levels increased substantially. At comparatively stable SM conditions, such as in the March 17th–11th pair, the satellite retrieval is less accurate. Even at

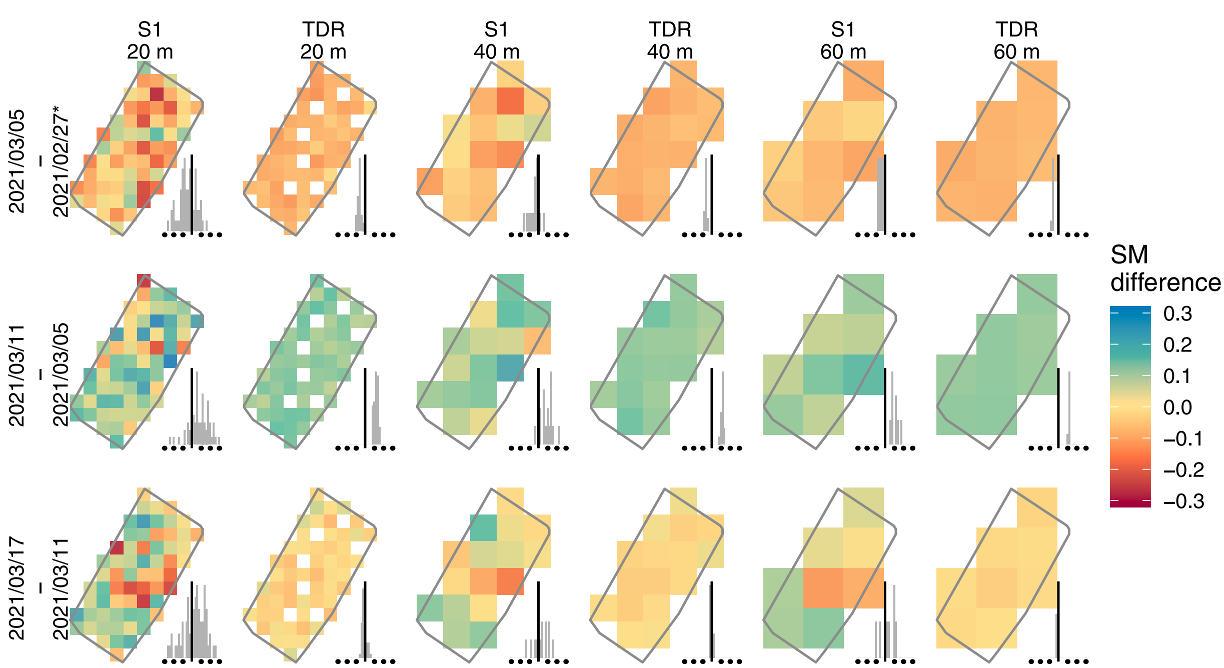

Fig. 11. Temporal difference between SM on subsequent field days in February and March 2021, at 20 m, 40 m, and 60 m resolution. Histograms show the distribution of values, with a vertical line at zero and tick marks at every 0.1.
*Due to a lack of in situ data on 2021-02-27, in situ data from 2021-02-26 are shown.

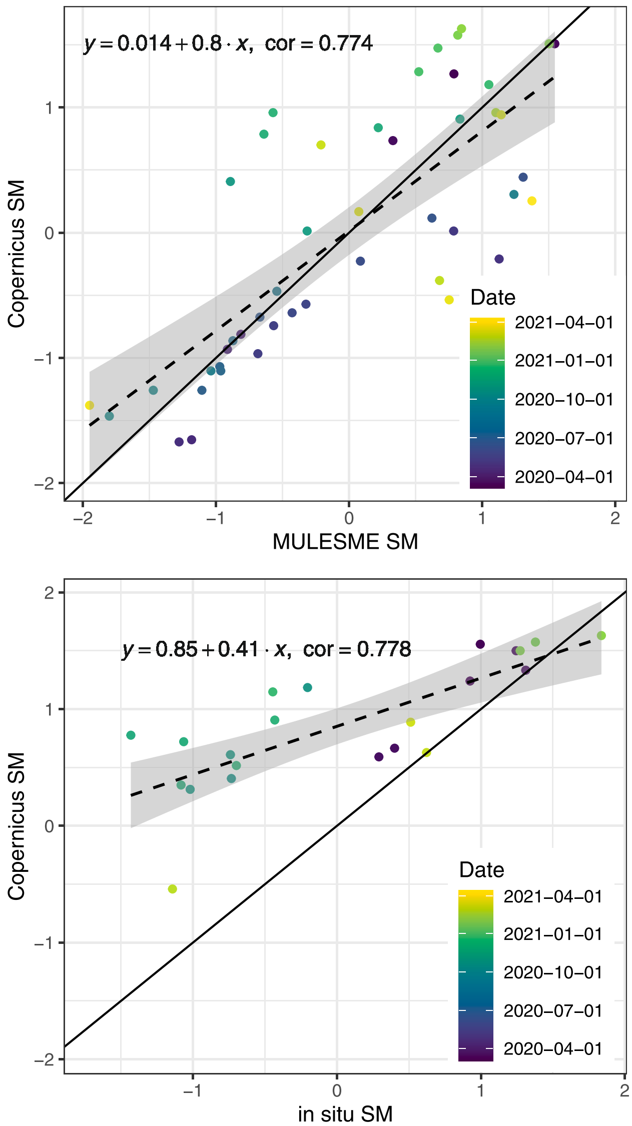

Fig. 12. A comparison between MULESME RO37 and Copernicus SM data at a 1 × 1 km scale (top) and in situ and Copernicus SM data (bottom) over the field.

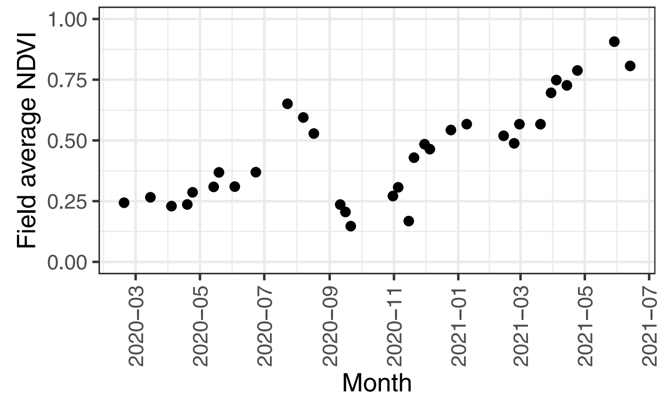

Fig. A.13. Time series of average NDVI in the studied agricultural field, where maize was grown in the first growing season, and winter wheat in the second.

Fig. A.14. DEM over the studied agricultural field, slowing a mild slope over the field.

the 60 m resolution, large S1 SM changes are visible on the studied field whereas no substantial change showed in the in situ data.

4.5. Copernicus data

To be able to put the MULESME analysis into context, we include an analysis of the CSSM dataset over our field (Fig. 12). The CSSM dataset has a spatial resolution of 1 × 1 km. Since our S1 retrieved SM data has a higher spatial resolution, we spatially aggregated the MULESME dataset to the same resolution and normalised them both to their minimum and maximum values. The top part of Fig. 12 shows the agreement between the two datasets in the 1 × 1 km pixel overlaying the field. This shows a good agreement and a strong temporal correlation (0.803) between both datasets. The bottom part of Fig. 12 shows the agreement between the Copernicus SM and the field average in situ SM measurements. These also showed a good agreement, with a temporal correlation of 0.778, compared to 0.583 between the 1 × 1 km MULESME and the field average. This is lower than the MULESME estimates at higher resolutions (Fig. 8(a)), indicating that further multilooking the data to lower resolutions reduces retrieval accuracies.

5. Discussion

We compared a SM dataset retrieved from S1 data with a high spatial resolution with a high spatial resolution field dataset with extended temporal coverage. This comparison showed that temporal SM variability was well reflected in the satellite data, although performance increased with decreasing spatial resolution (Fig. 8). Spatial performance behaved similarly, but r was generally low and ubRMSE was generally high (Fig. 9). Taking into account differences in performance dependent on field conditions, the optimal retrieval accuracy was finally identified at a 60 m resolution using the RO37 data (i.e. the equivalent of 36 looks of native S1 data). At that resolution, a good average temporal correlation (0.67, or 0.69 only taking into account significant r values) was found and sub-field SM variation could still be distinguished.

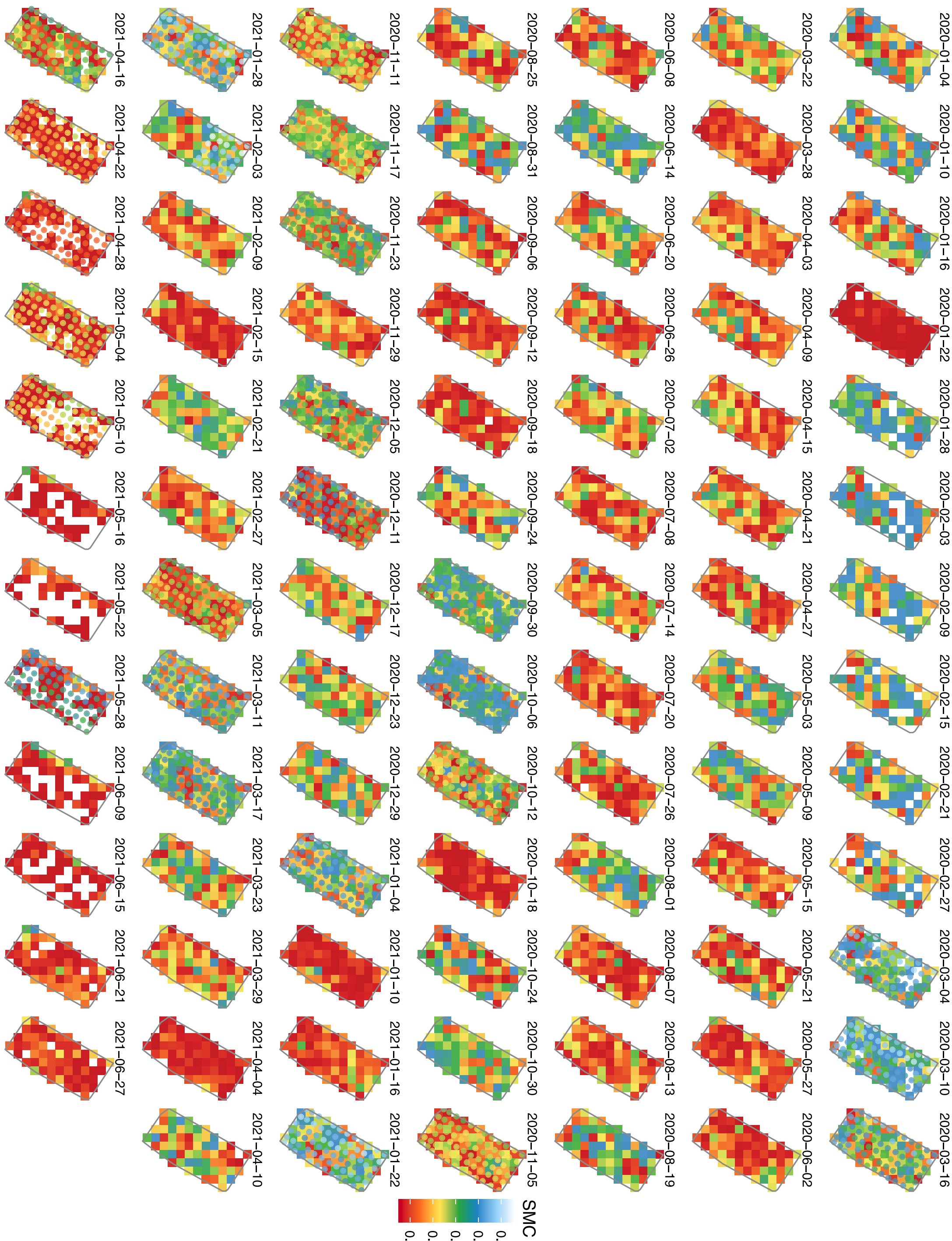

Fig. B.15. All RO37 SM retrievals at 20 m resolution, overlain with in situ TDR data.

Performance of the satellite dataset depended on the satellite orbit and on field conditions (Fig. 7), most notably on temperature, vegetation and wetness. The performance difference between the orbits could be caused by their different incidence angles (Palmisano et al., 2021). Frozen soils caused negative spatial correlation (Fig. 9) due to the inverse relationship between backscatter and SM under these conditions as compared to "normal" conditions (de Rosnay et al., 2006; Hallikainen et al., 1985). The presence of vegetation increased the bias of the S1 SM retrievals (Fig. 7), as previously found by for instance (Bindlish and Barros, 2001; Zhang et al., 2021; Yadav et al., 2020). However, the spatial correlation was barely affected by increased NDVI values, and the ubRMSE was even lower at higher NDVI values (Fig. 9). Based on the sudden decrease in estimated roughness during the same period (Fig. 5), it seems that the increase in performance is coincidental. Wheat attenuates backscatter especially at high incidence angles due to its geometry (Mattia et al., 2003), as does a decreasing moisture content that occurs simultaneously. Decreasing backscatter and hence decreasing moisture estimates are therefore likely caused by vegetation growth rather than decreasing moisture conditions, indicating that S1 SM estimates were unreliable in that period.

The case study showed that temporal variability could be described better when clear variations in SM existed. Unfortunately, since the study area was not irrigated, spatial variation in SM was limited

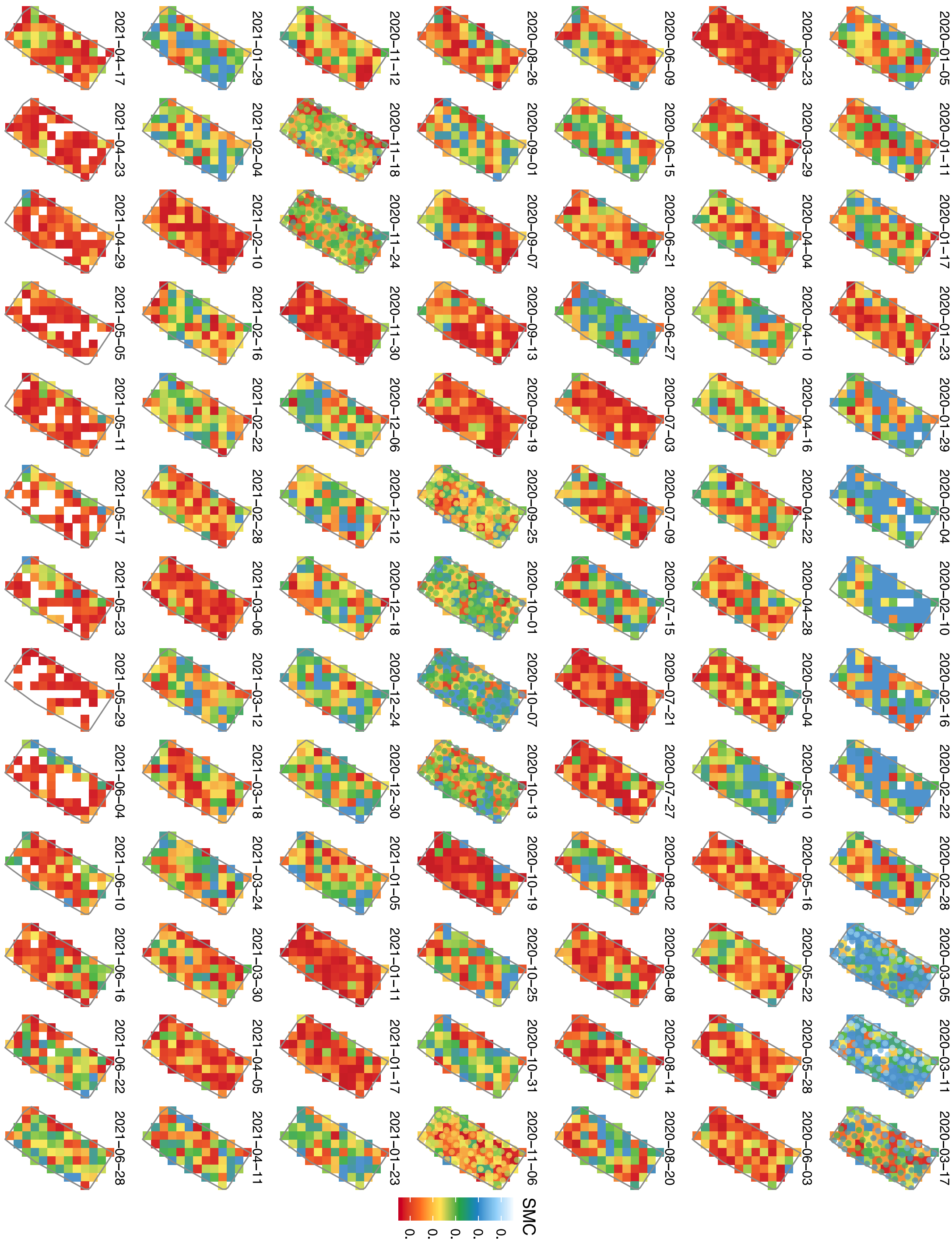

Fig. B.16. All RO139 SM retrievals at 20 m resolution, overlain with in situ TDR data.

(Fig. 6). Meanwhile, a large spatial variability existed in S1 SM, especially in images with a high spatial resolution. This indicates that the sub-field variation in SM is smaller than the spatial variation in the backscatter data. This high spatial variation is not caused by the retrieval algorithm, because the algorithm is pixel-based and so SM values do not depend on neighbouring pixels. The spatial variations in S1 SM were thus caused by speckle, indicating that at high spatial resolutions, the spatial signal is smaller than the noise. Speckle introduces spatially uncorrelated fluctuation, whereas it is quite correlated in time due to the small orbital tube of S1 (Torres et al., 2012). Hence, temporal variation in speckle is limited. This explains why temporal performance was better than the spatial performance. High spatial resolution S1 data thus contain information on temporal variability of SM that could be further exploited.

While speckle did influence SM retrievals at a high spatial resolution, a correlation with reference data as high as 1 is near to impossible because in situ data have their own uncertainties. Uncertainties in SM observations are a common issue: due to small-scale variations in SM caused by for instance local topography, heterogeneous soil properties and plant water uptake, point scale SM can be different from gridded SM (e.g. Western and Blöschl, 1999; Teuling et al., 2006; Famiglietti et al., 2008; Vereecken et al., 2008; Babaeian et al., 2019). The uncertainty of in situ SM observations makes it difficult to relate the in situ SM to the ground truth. Therefore the uncertainty was limited as much as possible by taking five measurements at each sampling location and by calibrating the data with volumetric soil samples.

The MULESME algorithm assumes that roughness in each pixel remains constant over the five considered backscatter images. The assumption of constant roughness always is a major part of a multitemporal algorithm, but the way this assumption is handled depends on the algorithm. Results from a second multitemporal algorithm (TU Wien) were therefore also compared to the in situ data. This analysis showed that the TU Wien algorithm results in higher temporal correlations than the MULESME dataset. At the same time, the MULESME dataset was able to accurately depict temporal SM variations at a much higher spatial resolution. In light of the high temporal correlation between the two products at a 1 × 1 km resolution, we believe that the use of a different SM retrieval algorithm for the present study would not have considerably affected the results.

The measurements presented in this paper were made in a moderate climate under varying moisture, meteorological and vegetation conditions. Since the entire range of valid SM conditions was observed, the chosen location for the field campaign had sufficient seasonality in moisture conditions, as well as sufficient different meteorological conditions and vegetation states. Finally, the studied field is a "normal" agricultural field by European standards in terms of size, slope and soil type. Because of these wide ranging conditions, conclusions from this study are expected to be valid under most conditions and perhaps even in other climatic zones.

6. Conclusion and outlook

A high spatial resolution SM dataset resulting from S1 backscatter data was used to explore the limits in spatial resolution of active microwave SM measurements. The performance of this 6-day dataset was evaluated with a closely spaced in situ SM data that was collected in a dedicated field campaign in Southeastern Luxembourg. This comparison showed that the optimal retrieval accuracy could be found at a 60 m resolution, equivalent to 36 looks on a native S1 spatial resolution: a good average temporal correlation was found and spatial variation could still be distinguished. Spatial correlation, on the other hand, was low, likely due to the limited spatial variability over the field. A case study under favourable field conditions did show that short-term SM variability could be captured on a 60 m resolution regardless of the low spatial correlation.

Though high spatial resolution SM data have been presented before, to the best of our knowledge, this is the first time that they were compared to an extensive in situ dataset whose spacing matches the S1 native spatial resolution. We demonstrated that high resolution backscatter intensity images can contain temporal information on SM at a spatial scale smaller than the field scale, and future research should focus on further exploiting this merit. Another path to explore would be an analysis on a larger scale, with larger spatial variability in SM, thereby also including other land cover types, soil types and soil textures. It would be interesting to study how large scale SM monitoring on high resolutions would compare to a similar analysis on lower resolutions. Sub-field variations might be of significant importance for the evolution of SM droughts and can thus be of interest for the drought community, as well as for precision agriculture applications.

CRediT authorship contribution statement

T.C. van Hateren: Conceptualization, Methodology, Software, Formal analysis, Investigation, Data curation, Writing – original draft, Visualisation. **M. Chini:** Conceptualization, Methodology, Writing – review & editing, Supervision. **P. Matgen:** Conceptualization, Methodology, Writing – review & editing, Supervision. **L. Pulvirenti:** Methodology, Software, Writing – review & editing. **N. Pierdicca:** Methodology, Software, Writing – review & editing. **A.J. Teuling:** Conceptualization, Methodology, Writing – review & editing, Supervision.

Declaration of competing interest

The authors declare that they have no known competing financial interests or personal relationships that could have appeared to influence the work reported in this paper.

Data availability

Data will be made available on request.

Acknowledgements

We thank the anonymous reviewers who have helped improve this manuscript.

Funding

This research was funded by the Fonds National de la Recherche Luxembourg (FNR), grant no. PRIDE15/10623093 – HYDRO-CSI.

Appendix A. Field conditions

See Figs. A.13 and A.14.

Appendix B. SM data

See Figs. B.15 and B.16.

References

Attarzadeh, R., Amini, J., Notarnicola, C., Greifeneder, F., 2018. Synergetic use of Sentinel-1 and Sentinel-2 data for soil moisture mapping at plot scale. Remote Sens. 10 (1285), http://dx.doi.org/10.3390/rs10081285.

Attema, E.P.W., Ulaby, F.T., 1978. Vegetation modeled as a water cloud. Radio Sci. 13, 357–364. http://dx.doi.org/10.1029/RS013i002p00357.

Babaeian, E., Sadeghi, M., Jones, S.B., Montzka, C., Vereecken, H., Tuller, M., 2019. Ground proximal, and satellite remote sensing of soil moisture. Rev. Geophys. 57, 530–616. http://dx.doi.org/10.1029/2018RG000618.

Balenzano, A., Mattia, F., Satalino, G., Davidson, M.W.J., 2011. Dense temporal series of C- and L-band SAR data for soil moisture retrieval over agricultural crops. IEEE J. Sel. Top. Appl. Earth Obs. Remote Sens. 4, http://dx.doi.org/10.1109/JSTARS.2010.2052916.

Bauer-Marschallinger, B., Freeman, V., Cao, S., Paulik, C., Schaufler, S., Stachl, T., Modanesi, S., Massari, C., Ciabatta, L., Brocca, L., Wagner, W., 2019. Toward global soil moisture monitoring with Sentinel-1: Harnessing assets and overcoming obstacles. IEEE Trans. Geosci. Remote Sens. 57, 520–539. http://dx.doi.org/10.1109/TGRS.2018.2858004.

Bierkens, M.F.P., Bell, V.A., Burek, P., Chaney, N., Condon, L.E., David, C.H., de Roo, A., Döll, P., Drost, N., Famiglietti, J.S., Flörke, M., Gochis, D.J., Houser, P., Hut, R., Keune, J., Kollet, S., Maxwell, R.M., Reager, J.T., Samaniego, L., Sudicky, E., Sutanudjaja, E.H., van de Giesen, N., Winsemius, H., Wood, E.F., 2015. Hyper-resolution global hydrological modelling: what is next? Hydrol. Process. 29, 310–320. http://dx.doi.org/10.1002/hyp.10391.

Bindlish, R., Barros, A.P., 2001. Parameterization of vegetation backscatter in radar-based, soil moisture estimation. Remote Sens. Environ. 76, 130–137. http://dx.doi.org/10.1016/S0034-4257(00)00200-5.

Bousbih, S., Zribi, M., Lili-Chabaane, Z., Baghdadi, N., El Hajj, M., Gao, Q., Mougenot, B., 2017. Potential of Sentinel-1 radar data for the assessment of soil and cereal cover parameters. Sensors 17 (11), 2617. http://dx.doi.org/10.3390/s17112617.

Chan, S., Hunt, R., Bindlish, R., Njoku, E., Kimball, J., Jackson, T., 2011. Ancillary Data Report for Vegetation Water Content. Technical Report SMAP Project Document #D53061, JPL.

Choker, M., Baghdadi, N., Zribi, M., El Hajj, M., Paloscia, S., Verhoest, N.E.C., Lievens, H., Mattia, F., 2017. Evaluation of the Oh, Dubois and IEM backscatter models using a large dataset of SAR data and experimental soil measurements. Water 9, 38. http://dx.doi.org/10.3390/w9010038.

Colliander, A., Cosh, M.H., Misra, S., Jackson, T.J., Crow, W.T., Powers, J., McNairn, H., Bullock, P., Berg, A., Magagi, R., Gao, Y., Bindlish, R., Williamson, R., Ramos, I., Latham, B., O'Neill, P., Yueh, S., 2019. Comparison of high-resolution airborne soil moisture retrievals to SMAP soil moisture during the SMAP validation experiment 2016 (SMAPVEX16). Remote Sens. Environ. 227, 137–150. http://dx.doi.org/10.1016/j.rse.2019.04.004.

Colliander, A., Jackson, T.J., Bindlish, R., Chan, S., Das, N., Kim, S.B., Cosh, M.H., Dunbar, R.S., Dang, L., Pashaian, L., Asanuma, J., Aida, K., Berg, A., Rowlandson, T., Bosch, D., Caldwell, T., Caylor, K., Goodrich, D., al Jassar, H., Lopez-Baeza, E., Martínez-Fernández, J., González-Zamora, A., Livingston, S., McNairn, H., Pacheco, A., Moghaddam, M., Montzka, C., Notarnicola, C., Niedrist, G., Pellarin, T., Prueger, J., Pulliainen, J., Rautiainen, K., Ramos, J., Seyfried, M., Starks, P., Su, Z., Zeng, Y., van der Velde, R., Thibeault, M., Dorigo, W., Vreugdenhil, M., Walker, J.P., Wu, X., Monerris, A., O'Neill, P.E., Entekhabi, D., Njoku, E.G., Yueh, S., 2017. Validation of SMAP surface soil moisture products with core validation sites. Remote Sens. Environ. 191, 215–231. http://dx.doi.org/10.1016/j.rse.2017.01.021.

Colliander, A., Jackson, T., McNairn, H., Chazanoff, S., Dinardo, S., Latham, B., O'Dwyer, I., Chun, W., Yueh, S., Njoku, E., 2015. Comparison of airborne passive and active L-band system (PALS) brightness temperature measurements to SMOS observations during the SMAP validation experiment 2012 (SMAPVEX12). IEEE Geosci. Remote Sens. Lett. 12, 801–805. http://dx.doi.org/10.1109/LGRS.2014.2362889.

Crow, W.T., Berg, A.A., Cosh, M.H., Loew, A., Mohanty, B.P., Panciera, R., de Rosnay, P., Ryu, D., Walker, J.P., 2012. Upscaling sparse ground-based soil moisture observations for the validation of coarse-resolution satellite soil moisture products. Rev. Geophys. 50, http://dx.doi.org/10.1029/2011RG000372.

de Rosnay, P., Calvet, J.C., Kerr, Y., Wigneron, J.P., Lemaître, F., Escorihuela, M.J., Sabater, J.M., Saleh, K., Barrié, G., Coret, L., Cherel, G., Dedieu, G., Durbe, R., Fritz, N.E.D., Froissard, F., Hoedjes, J., Kruszewski, A., Lavenu, F., Suquia, D., Waldteufel, P., 2006. SMOSREX: A long term field campaign experiment for soil moisture and land surface processes remote sensing. Remote Sens. Environ. 102, 377–389. http://dx.doi.org/10.1016/j.rse.2006.02.021.

Del Frate, F., Ferrazzoli, P., Schiavon, G., 2003. Retrieving soil moisture and agricultural variables by microwave radiometry using neural networks. Remote Sens. Environ. 84, 174–183. http://dx.doi.org/10.1016/S0034-4257(02)00105-0.

Dorigo, W., Himmelbauer, I., Aberer, D., Schremmer, L., Petrakovic, I., Zappa, L., Preimesberger, W., Xaver, A., Annor, F., Ardö, J., Baldocchi, D., Bitelli, M., Blöschl, G., Bogena, H., Brocca, L., Calvet, J.C., Camarero, J.J., Capello, G., Choi, M., Cosh, M.C., van de Giesen, N., Hajdu, I., Ikonen, J., Jensen, K.H., Kanniah, K.D., de Kat, I., Kirchengast, G., Kumar Rai, P., Kyrouac, J., Larson, K., Liu, S., Loew, A., Moghaddam, M., Martínez Fernández, J., Mattar Bader, C., Morbidelli, R., Musial, J.P., Osenga, E., Palecki, M.A., Pellarin, T., Petropoulos, G.P., Pfeil, I., Powers, J., Robock, A., Rüdiger, C., Rummel, U., Strobel, M., Su, Z., Sullivan, R., Tagesson, T., Varlagin, A., Vreugdenhil, M., Walker, J., Wen, J., Wenger, F., Wigneron, J.P., Woods, M., Yang, K., Zeng, Y., Zhang, X., Zreda, M., Dietrich, S., Gruber, A., van Oevelen, P., Wagner, W., Scipal, K., Drusch, M., Sabia, R., 2021. The international soil moisture network: serving Earth system science for over a decade. Hydrol. Earth Syst. Sci. 25, 5749–5804. http://dx.doi.org/10.5194/hess-25-5749-2021.

El Hajj, M., Baghdadi, N., Zribi, M., Bazzi, H., 2017. Synergic use of Sentinel-1 and Sentinel-2 images for operational soil moisture mapping at high spatial resolution over agricultural areas. Remote Sens. 9, 1292. http://dx.doi.org/10.3390/rs9121292.

Elshorbagy, A., Parasuraman, K., 2008. On the relevance of using artificial neural networks for estimating soil moisture content. J. Hydrol. 362, 1–18. http://dx.doi.org/10.1016/j.jhydrol.2008.08.012.

Entekhabi, D., Reichle, R.H., Koster, R.D., Crow, W.T., 2010. Performance metrics for soil moisture retrievals and application requirements. J. Hydrometeorol. 11, 832–840. http://dx.doi.org/10.1175/2010JHM1223.1, section: Journal of Hydrometeorology.

EROS, 2017. Shuttle Radar Topography Mission (SRTM) 1 arc-second global. http://dx.doi.org/10.5066/F7PR7TFT, URL: https://www.usgs.gov/centers/eros/science/usgs-eros-archive-digital-elevation-shuttle-radar-topography-mission-srtm-1-arc, medium: tiff Type: dataset.

ESAS̃entinelÕnline, 2023. IW GRD resolutions - Sentinel-1 SAR technical guide. URL: https://sentinels.copernicus.eu/web/sentinel/technical-guides/sentinel-1-sar/products-algorithms/level-1-algorithms/ground-range-detected/iw.

Ezzahar, J., Ouaadi, N., Zribi, M., Elfarkh, J., Aouade, G., Khabba, S., Er-Raki, S., Chehbouni, A., Jarlan, L., 2020. Evaluation of backscattering models and support vector machine for the retrieval of bare soil moisture from Sentinel-1 data. Remote Sens. 12 (72), http://dx.doi.org/10.3390/rs12010072.

Famiglietti, J.S., Ryu, D., Berg, A.A., Rodell, M., Jackson, T.J., 2008. Field observations of soil moisture variability across scales. Water Resour. Res. 44, http://dx.doi.org/10.1029/2006WR005804.

Fung, A., Li, Z., Chen, K., 1992. Backscattering from a randomly rough dielectric surface. IEEE Trans. Geosci. Remote Sens. 30, 356–369. http://dx.doi.org/10.1109/36.134085, conference Name: IEEE Transactions on Geoscience and Remote Sensing.

Gruber, A., De Lannoy, G., Albergel, C., Al-Yaari, A., Brocca, L., Calvet, J.C., Colliander, A., Cosh, M., Crow, W., Dorigo, W., Draper, C., Hirschi, M., Kerr, Y., Konings, A., Lahoz, W., McColl, K., Montzka, C., Muñoz-Sabater, J., Peng, J., Reichle, R., Richaume, P., Rüdiger, T., van der Schalie, R., Wigneron, J.P., Wagner, W., 2020. Validation practices for satellite soil moisture retrievals: What are (the) errors? Remote Sens. Environ. 244, 111806. http://dx.doi.org/10.1016/j.rse.2020.111806.

Hachani, A., Ouessar, M., Paloscia, S., Santi, E., Pettinato, S., 2019. Soil moisture retrieval from Sentinel-1 acquisitions in an arid environment in Tunisia: application of Artificial Neural Networks techniques. Int. J. Remote Sens. 40, 9159–9180. http://dx.doi.org/10.1080/01431161.2019.1629503.

Hallikainen, M.T., Ulaby, F.T., Dobson, M.C., El-rayes, M.A., Wu, L.k., 1985. Microwave dielectric behavior of wet soil-Part 1: Empirical models and experimental observations. IEEE Trans. Geosci. Remote Sens. GE-23, 25–34. http://dx.doi.org/10.1109/TGRS.1985.289497, conference Name: IEEE Transactions on Geoscience and Remote Sensing.

Hostache, R., Rains, D., Mallick, K., Chini, M., Pelich, R., Lievens, H., Fenicia, F., Corato, G., Verhoest, N.E.C., Matgen, P., 2020. Assimilation of Soil Moisture and Ocean Salinity (SMOS) brightness temperature into a large-scale distributed conceptual hydrological model to improve soil moisture predictions: the Murray–Darling basin in Australia as a test case. Hydrol. Earth Syst. Sci. 24, 4793–4812. http://dx.doi.org/10.5194/hess-24-4793-2020.

Kim, S.B., Moghaddam, M., Tsang, L., Burgin, M., Xu, X., Njoku, E.G., 2014. Models of L-band radar backscattering coefficients over global terrain for soil moisture retrieval. IEEE Trans. Geosci. Remote Sens. 52, 1381–1396. http://dx.doi.org/10.1109/TGRS.2013.2250980, conference Name: IEEE Transactions on Geoscience and Remote Sensing.

Lagasio, M., Parodi, A., Pulvirenti, L., Meroni, A.N., Boni, G., Pierdicca, N., Marzano, F.S., Luini, L., Venuti, G., Realini, E., Gatti, A., Tagliaferro, G., Barindelli, S., Monti Guarnieri, A., Goga, K., Terzo, O., Rucci, A., Passera, E., Kranzlmueller, D., Rommen, B., 2019a. A synergistic use of a high-resolution numerical weather prediction model and high-resolution earth observation products to improve precipitation forecast. Remote Sens. 11 (2387), http://dx.doi.org/10.3390/rs11202387.

Lagasio, M., Pulvirenti, L., Parodi, A., Boni, G., Pierdicca, N., Venuti, G., Realini, E., Tagliaferro, G., Barindelli, S., Rommen, B., 2019b. Effect of the ingestion in the WRF model of different Sentinel-derived and GNSS-derived products: analysis of the forecasts of a high impact weather event. European Journal of Remote Sensing 52, 16–33. http://dx.doi.org/10.1080/22797254.2019.1642799.

Lee, J.S., 1986. Speckle suppression and analysis for synthetic aperture radar images. Opt. Eng. 25, 636–643. http://dx.doi.org/10.1117/12.7973877.

Lee, J.H., Budhathoki, S., Lindenschmidt, K.E., 2021. Stochastic bias correction for RADARSAT-2 soil moisture retrieved over vegetated areas. Geocarto Int. 1–14. http://dx.doi.org/10.1080/10106049.2021.2017009, publisher: Taylor & Francis.

Matgen, P., Heitz, S., Hasenauer, S., Hissler, C., Brocca, L., Hoffmann, L., Wagner, W., Savenije, H.H.G., 2012. On the potential of MetOp ASCAT-derived soil wetness indices as a new aperture for hydrological monitoring and prediction: a field evaluation over Luxembourg. Hydrol. Process. 26, 2346–2359. http://dx.doi.org/10.1002/hyp.8316.

Mattia, F., Le Toan, T., Picard, G., Posa, F., D'Alessio, A., Notarnicola, C., Gatti, A., Rinaldi, M., Satalino, G., Pasquariello, G., 2003. Multitemporal C-band radar measurements on wheat fields. IEEE Trans. Geosci. Remote Sens. 41, 1551–1560. http://dx.doi.org/10.1109/TGRS.2003.813531, conference Name: IEEE Transactions on Geoscience and Remote Sensing.

Mattia, F., Satalino, G., Pauwels, V.R.N., Loew, A., 2009. Soil moisture retrieval through a merging of multi-temporal L-band SAR data and hydrologic modelling. Hydrol. Earth Syst. Sci. 13, 343–356. http://dx.doi.org/10.5194/hess-13-343-2009, publisher: Copernicus GmbH.

Miralles, D.G., Gentine, P., Seneviratne, S.I., Teuling, A.J., 2019. Land–atmospheric feedbacks during droughts and heatwaves: state of the science and current challenges. Ann. New York Acad. Sci. 1436, 19–35. http://dx.doi.org/10.1111/nyas.13912.

Oh, Y., 2004. Quantitative retrieval of soil moisture content and surface roughness from multipolarized radar observations of bare soil surfaces. IEEE Trans. Geosci. Remote Sens. 42, 596–601. http://dx.doi.org/10.1109/TGRS.2003.821065.

Palmisano, D., Mattia, F., Balenzano, A., Satalino, G., Pierdicca, N., Guarnieri, A.V.M., 2021. Sentinel-1 sensitivity to soil moisture at high incidence angle and the impact on retrieval over seasonal crops. IEEE Trans. Geosci. Remote Sens. 1–14. http://dx.doi.org/10.1109/TGRS.2020.3033887, tex.ids: palmisano2021 Conference Name: IEEE Transactions on Geoscience and Remote Sensing.

Peng, J., Albergel, C., Balenzano, A., Brocca, L., Cartus, O., Cosh, M.H., Crow, W.T., Dabrowska-Zielinska, K., Dadson, S., Davidson, M.W.J., de Rosnay, P., Dorigo, W., Gruber, A., Hagemann, S., Hirschi, M., Kerr, Y.H., Lovergine, F., Mahecha, M.D., Marzahn, P., Mattia, F., Musial, J.P., Preuschmann, S., Reichle, R.H., Satalino, G., Silgram, M., van Bodegom, P.M., Verhoest, N.E.C., Wagner, W., Walker, J.P., Wegmüller, A., 2021. A roadmap for high-resolution satellite soil moisture applications – confronting product characteristics with user requirements. Remote Sens. Environ. 252, 112162. http://dx.doi.org/10.1016/j.rse.2020.112162.

Pierdicca, N., Pulvirenti, L., Pace, G., 2014. A prototype software package to retrieve soil moisture from Sentinel-1 data by using a Bayesian multitemporal algorithm. IEEE J. Sel. Top. Appl. Earth Obs. Remote Sens. 7, 153–166. http://dx.doi.org/10.1109/JSTARS.2013.2257698, conference Name: IEEE Journal of Selected Topics in Applied Earth Observations and Remote Sensing.

Pulvirenti, L., Squicciarino, G., Cenci, L., Boni, G., Pierdicca, N., Chini, M., Versace, C., Campanella, P., 2018. A surface soil moisture mapping service at national (Italian) scale based on Sentinel-1 data. Environ. Model. Softw. 102, 13–28. http://dx.doi.org/10.1016/j.envsoft.2017.12.022.

Reichle, R.H., Koster, R.D., Liu, P., Mahanama, S.P.P., Njoku, E.G., Owe, M., 2007. Comparison and assimilation of global soil moisture retrievals from the Advanced Microwave Scanning Radiometer for the Earth Observing System (AMSR-E) and the Scanning Multichannel Microwave Radiometer (SMMR). J. Geophys. Res.: Atmos. 112, http://dx.doi.org/10.1029/2006JD008033.

Schönbrodt-Stitt S. Ahmadian, N., Kurtenbach, M., Conrad, C., Romano, N., Bogena, H.R., Vereecken, H., Nasta, P., 2021. Statistical exploration of Sentinel-1 data, terrain parameters, and in-situ data for estimating the near-surface soil moisture in a Mediterranean agroecosystem. Front. Water 3, 75. http://dx.doi.org/10.3389/frwa.2021.655837.

Seneviratne, S.I., Corti, T., Davin, E.L., Hirschi, M., Jaeger, E.B., Lehner, I., Orlowsky, B., Teuling, A.J., 2010. Investigating soil moisture–climate interactions in a changing climate: A review. Earth-Sci. Rev. 99, 125–161. http://dx.doi.org/10.1016/j.earscirev.2010.02.004.

Teuling, A.J., 2018. A hot future for European droughts. Nature Clim. Change 8, 364–365. http://dx.doi.org/10.1038/s41558-018-0154-5.

Teuling, A.J., Uijlenhoet, R., Hupet, F., van Loon, E.E., Troch, P.A., 2006. Estimating spatial mean root-zone soil moisture from point-scale observations. Hydrol. Earth Syst. Sci. 10, 755–767. http://dx.doi.org/10.5194/hess-10-755-2006.

Torres, R., Snoeij, P., Geudtner, D., Bibby, D., Davidson, M., Attema, E., Potin, P., Rommen, B., Floury, N., Brown, M., Traver, I.N., Deghaye, P., Duesmann, B., Rosich, B., Miranda, N., Bruno, C., L'Abbate, M., Croci, R., Pietropaolo, A., Huchler, M., Rostan, F., 2012. GMES Sentinel-1 mission. Remote Sens. Environ. 120, 9–24. http://dx.doi.org/10.1016/j.rse.2011.05.028.

Tripathi, A., Tiwari, R.K., 2020. Synergetic utilization of Sentinel-1 SAR and Sentinel-2 optical remote sensing data for surface soil moisture estimation for Rupnagar, Punjab, India. Geocarto Int. 1–22. http://dx.doi.org/10.1080/10106049.2020.1815865.

van Hateren, T.C., Chini, M., Matgen, P., Pulvirenti, L., Pierdicca, N., Teuling, A.J., 2023. On the use of native resolution backscatter intensity data for optimal soil moisture retrieval. IEEE Geosci. Remote Sens. Lett. 1. http://dx.doi.org/10.1109/LGRS.2023.3264732.

Vereecken, H., Huisman, J.A., Bogena, H., Vanderborght, J., Vrugt, J.A., Hopmans, J.W., 2008. On the value of soil moisture measurements in vadose zone hydrology: A review. Water Resour. Res. 44, http://dx.doi.org/10.1029/2008WR006829.

Vereecken, H., Huisman, J.A., Pachepsky, Y., Montzka, C., Kruk, J.van.der., Bogena, H., Weihermüller, M., Martinez, G., Vanderborght, J., 2014. On the spatio-temporal dynamics of soil moisture at the field scale. J. Hydrol. 516, 76–96. http://dx.doi.org/10.1016/j.jhydrol.2013.11.061.

Vergopolan, N., Xiong, S., Estes, L., Wanders, N., Chaney, N.W., Wood, E.F., Konar, M., Caylor, K., Beck, H.E., Gatti, N., Evans, T., Sheffield, J., 2021. Field-scale soil moisture bridges the spatial-scale gap between drought monitoring and agricultural yields. Hydrol. Earth Syst. Sci. 25, 1827–1847. http://dx.doi.org/10.5194/hess-25-1827-2021.

Wagner, W., Lemoine, G., Rott, H., 1999. A method for estimating soil moisture from ERS scatterometer and soil data. Remote Sens. Environ. 70, 191–207. http://dx.doi.org/10.1016/S0034-4257(99)00036-X.

Wang, H., Magagi, R., Goïta, K., 2018. Potential of a two-component polarimetric decomposition at C-band for soil moisture retrieval over agricultural fields. Remote Sens. Environ. 217, 38–51. http://dx.doi.org/10.1016/j.rse.2018.08.003.

Western, A.W., Blöschl, G., 1999. On the spatial scaling of soil moisture. J. Hydrol. 217, 203–224. http://dx.doi.org/10.1016/S0022-1694(98)00232-7.

Wood, E.F., Roundy, J.K., Troy, T.J., van Beek, L.P.H., Bierkens, M.F.P., Blyth, E., de Roo, A., Döll, P., Ek, M., Famiglietti, J., Gochis, D., van de Giesen, N., Houser, P., Jaffé, P.R., Kollet, S., Lehner, B., Lettenmaier, D.P., Peters-Lidard, C., Sivapalan, M., Sheffield, J., Wade, A., Whitehead, P., 2011. Hyperresolution global land surface modeling: Meeting a grand challenge for monitoring Earth's terrestrial water. Water Resour. Res. 47, http://dx.doi.org/10.1029/2010WR010090.

Yadav, V.P., Prasad, R., Bala, R., Vishwakarma, A.K., 2020. An improved inversion algorithm for spatio-temporal retrieval of soil moisture through modified water cloud model using C- band Sentinel-1A SAR data. Comput. Electron. Agric. 173, 105447. http://dx.doi.org/10.1016/j.compag.2020.105447.

Zhang, M., Lang, F., Zheng, N., 2021. Soil moisture retrieval during the wheat growth cycle using SAR and optical satellite data. Water 13 (135), http://dx.doi.org/10.3390/w13020135.

Zhu, L., Walker, J.P., Shen, X., 2020. Stochastic ensemble methods for multi-SAR-mission soil moisture retrieval. Remote Sens. Environ. 251, 112099. http://dx.doi.org/10.1016/j.rse.2020.112099.

Zhu, L., Walker, J.P., Tsang, L., Huang, H., Ye, N., Rüdiger, C., 2019. Soil moisture retrieval from time series multi-angular radar data using a dry down constraint. Remote Sens. Environ. 231, 111237. http://dx.doi.org/10.1016/j.rse.2019.111237.